Electronic Supplementary Material (ESI) for ChemComm. This journal is © The Royal Society of Chemistry 2022

Supporting Information for

Hydroxyl Radical-dominated Selective Oxidation of Ethylbenzene over a Photoactive Polyoxometalate-based Metal-organic Framework

Jiachen Jiao,[a] Ting Zhang,[a] Jiangbo Xu,[a] Kaixin Guo,[a] Jie Li,[a,b] Qiuxia Han*

[a]Henan Key Laboratory of Polyoxometalate Chemistry, Institute of Molecular and Crystal Engineering, College of Chemistry and Chemical Engineering, Henan University, Kaifeng 475004, PR China
[b]School of Chemistry & Chemical Engineering, Zhoukou Normal University, Zhoukou, Henan 466001, P. R. China

*Corresponding author. E-mail address: hdhqx@henu.edu.cn

Content:

Materials and Physical Measurements

All reagents were commercially purchased and used without further purification. $K_5BW_{12}O_{40}\cdot 5H_2O$ was prepared according to the literature and characterized by IR spectroscopy.[s1] The elemental analyses of C, H, and N were performed on a Vario EL III elemental analyzer. The infrared spectra (IR) were recorded from a sample powder palletized with KBr on a Nicolet170 SXFT-IR spectrometer over a range of 4000–400 cm^{-1}. Powder X-ray diffraction (PXRD) data were obtained on a Rigaku Model D/Max-2400 X-ray diffractometer with a sealed copper tube (λ = 1.54178 Å). Water contents were determined by TG analyses on a Mettler-Toledo TGA/SDTA 851^e instrument with a heating rate of 10 °C min^{-1} heated from 25 to 1000 °C under nitrogen. Inductively Coupled Plasma (ICP) of Cu, B, and W analyses were performed on a Jarrel-AshJ-A1100 spectrometer. The solid UV–Vis spectrum was carried out on UV-540 ultraviolet-visible spectrophotometer in the range of 200–800 nm at room temperature. The photocatalytic reduction reactions were monitored by WATTCAS Parallel Light Reactor (WP-TEC-1020HSL) with 10 W 365 nm LED. Electrochemical testing experiments were measured by CHI-660E (Shanghai Chenhua Instrument Co., China) which has a three-electrode experimental. The products were further determined by using the Agilent technologies 8860B GC and mass spectrometer Agilent technologies 5975C as the detector. Photoluminescence properties were explored on an EDINBURGH FLS 980 fluorescence spectrophotometer equipped with a 300 W xenon lamp.

Synthesis of 1

$[Cu^{I}_{3}(H_2O)_6(TPT)_2][H_2BW_{12}O_{40}]\cdot 28H_2O$ (1): $K_5BW_{12}O_{40}\cdot 5H_2O$ (90 mg, 0.03 mmol), $Cu(NO_3)_2\cdot 3H_2O$ (185 mg, 0.77 mmol), and TPT (18.5 mg, 0.06 mmol) were mixed in 4 mL of water and 2 mL of methanol solution at pH 2.3. The resultant mixture was stirred for 12 h, then sealed in a 25 mL Teflon-lined autoclave, and maintained at 130 °C for 4 days. After cooling the autoclave to room temperature, Grass-green polyhedral sphere crystals were separated, washed with water, and air-dried. The crystals were obtained with a good yield of 80% (Based on $K_5BW_{12}O_{40}\cdot 5H_2O$). Calcd for $C_{36}H_{92}BCu_3N_{12}O_{74}W_{12}$: Cu 4.45, W 51.49, C 10.09, H 2.16, N 3.92; Found: Cu 4.58, W 52.14, C 9.90, H 1.98, N 3.85.

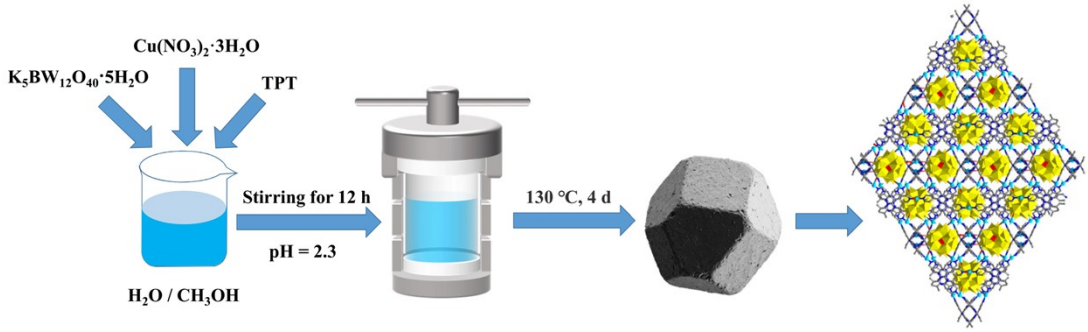

Fig. S1 Synthetic Process of **1.**

Electrochemical Measurements

All electrochemical tests were collected from an electrochemical workstation (CHI660E, Chenhua Instrument, Shanghai, China) in a standard three-electrode system with the photocatalyst-coated ITO as the working electrode, Platinum Wire as the counter electrode, and an Ag/AgCl as a reference electrode. A 300 W xenon lamp was used as the light source. A 0.1 M Na_2SO_4 solution was used as an electrolyte. The catalyst (10 mg) was added into a mixed solution with 700 μL ethanol and 200 μL of deionized water, and the working electrodes were prepared by dropping the suspension (80 μL) and 40 μL Nafion (Nafion: ethanol = 1:3) onto the surface of an ITO plate with an area of 1 cm^{-2}.

Single-crystal X-ray Crystallography

A good single crystal of **1** with dimensions of 0.22 × 0.15 × 0.12 mm^3 was prudentially picked under an optical microscope and sealed to a glass tube closed at both ends. The data of **1** was collected on a Bruker D8 VENTURE PHOTON II CCD diffractometer with graphite-monochromated Mo Kα (λ = 0.71073 Å) at 150 K using SAINT and SMART programs. Using Olex2,[s2] the structure was solved with the ShelXT structure solution program using Intrinsic Phasing and refined with the ShelXL refinement package using Least Squares minimisation.[s3] All the atoms were refined anisotropically in the last refinement cycle. H atoms were fixed in calculated positions and then refined using a riding model.

Highly disordered solvent was located in the structures. SQUEEZE (via Solvent Mask) was used to remove the contributions of some 1107 electrons from the reflection file. All of them are directly included in the molecular formula. This is consistent with the presence of 28[H2O] per formula unit which account for 1120 electrons. Therefore, there are 28[H2O] molecules were added to the chemical formulas. The CCDC number of **1** is 2233453. Crystallographic data and structure refinements for **1** are listed in **Table S1**.

Table S1 Crystal Data and Structure Refinement for **1**.

	1
Empirical formula	$C_{36}H_{92}BCu_3N_{12}O_{74}W_{12}$
Formula weight	4284.6812
Crystal system	Cubic
Space group	Pn-3
Temperature/K	150
$a = b = c$/Å	20.823(3)
α□□□β□□□γ□□□	90
V / Å^3	9029(4)
Z	4
Dcalcd / g cm^{-3}	2.774
F(000)	6688.0
μ / mm^{-1}	15.988
Crystal size / mm^3	0.11 × 0.08 × 0.06
2Θ range for data collection / °	4.792 to 50.162
Refl. collected / unique	24275/2685 [Rint=0.0624]
Index ranges	-23 ≤ h ≤ 24, -14 ≤ k ≤ 24, -23 ≤ l ≤ 23
GOF	1.021
R_1[a], wR_2[b] [$I > 2\sigma(I)$]	0.0563, 0.1322
R_1, wR_2 [all data]	0.0717, 0.1473
diff peak and hole, eÅ^{-3}	2.23 / -2.97

[a] $R_1 = \sum||Fo| - |Fc||/\sum|Fo|$, [b] $wR_2 = [\sum w(Fo^2 - Fc^2)^2/\sum w(Fo^2)^2]^{1/2}$; w = $1/[\sigma^2(Fo^2) + (xP)^2 + yP]$, P= $(Fo^2 + 2Fc^2)/3$, where x = 0.0365, y = 256.9678 for **1**.

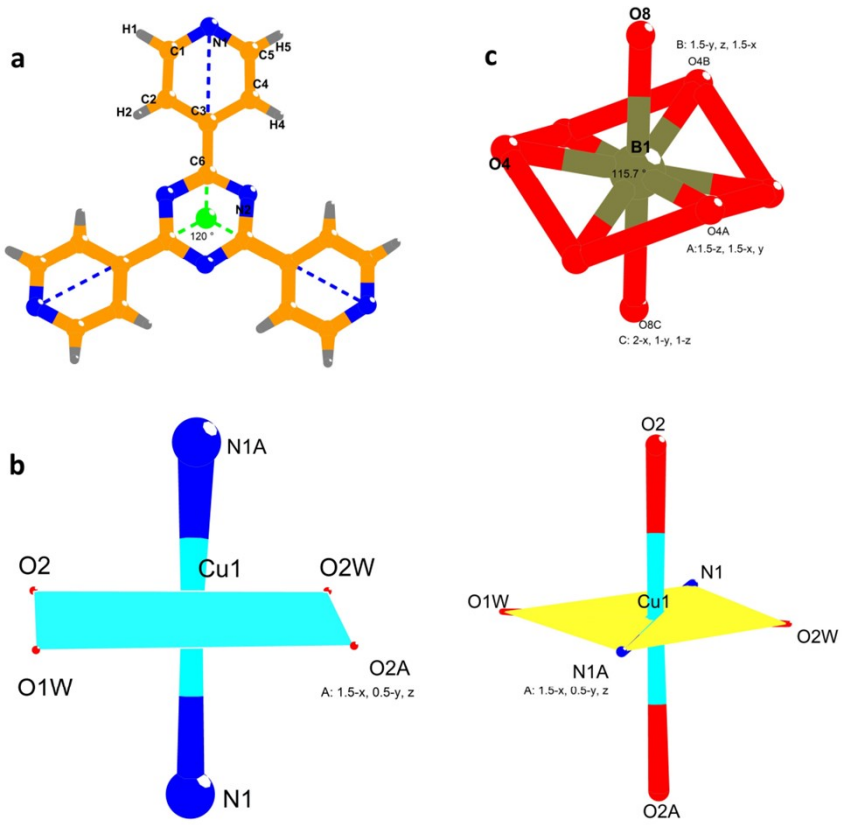

Fig. S2 (a) The threefold rotational axis in TPT ligand. (b) Two mirror planes: one which lies in the plane defined by the Cu1, O1W, O2W, O2 and O2A, the other that lies in the plane defined by the Cu1, O1W, O2W, N1 and N1A (A=1.5-x, 0.5-y, z). (c) B1 locating at an inversion center and a threefold rotational axis through B1 and O8.

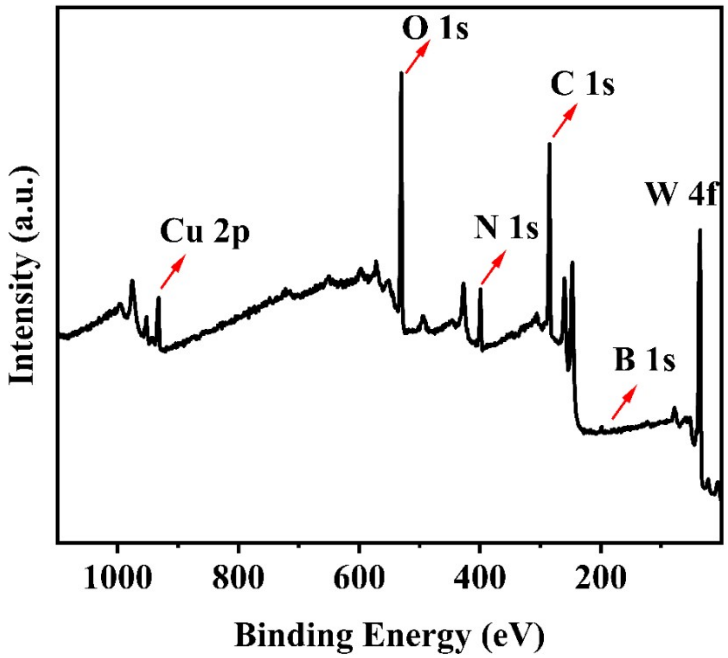

Fig. S3 The XPS survey spectra of fresh sample of **1**.

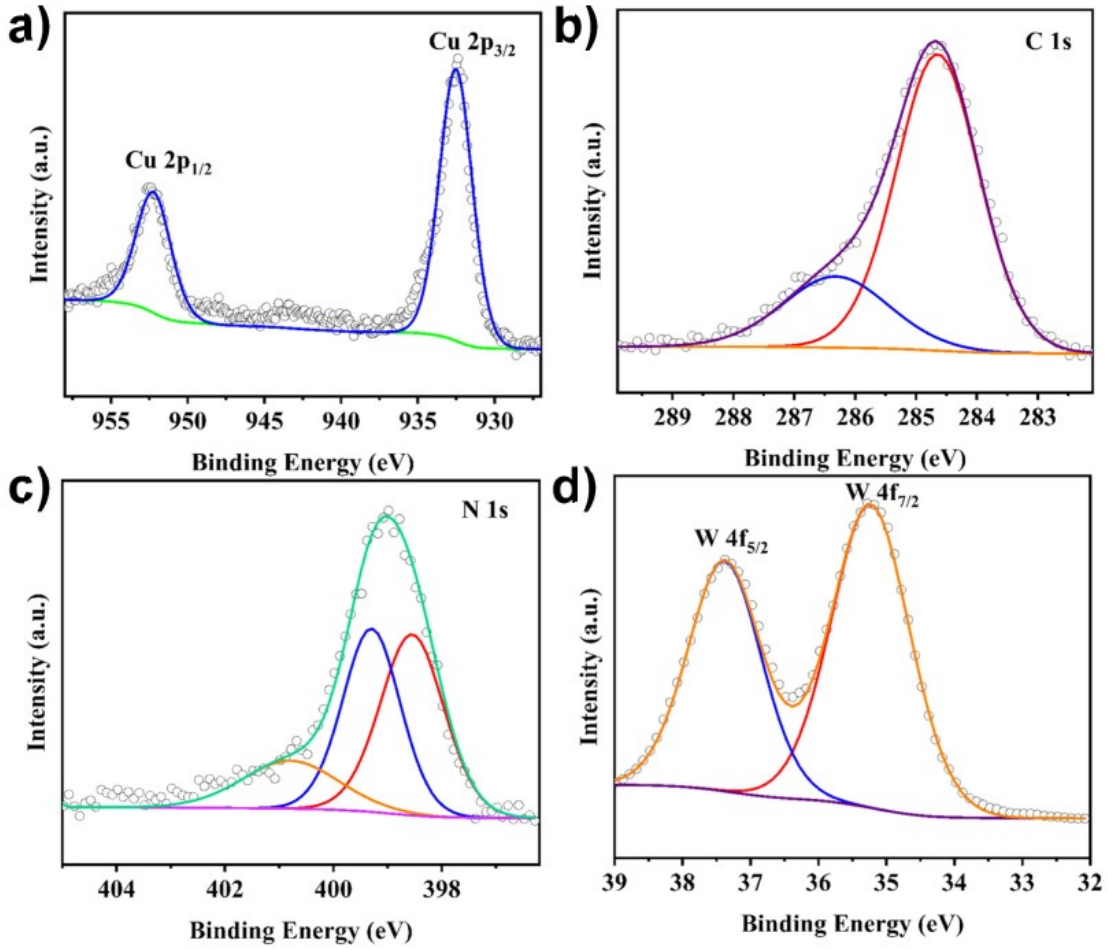

Fig. S4 The high-resolution XPS spectra of **1**: (a) Cu 2p, (b) C 1s, (c) N 1s (d) W 4f.

The deconvolution of the C 1s spectrum into two peaks of binding energy 284.8 and 286.4 eV corresponds to the pyridine ring and center ring in TPT, respectively. Meanwhile, the three peaks of nitrogen spectra at 398.6, 399.3, and 400.8 eV, represent the pyridine ring, the center ring, and the protonated N in TPT. The W 4f signal exhibits two peaks at 37.4 eV ($4f_{5/2}$) and 35.2 eV ($4f_{7/2}$) that are assigned to the W^{6+} environment. Two peaks at 932.5 and 952.0 eV in the Cu 2p region of **1** should be assigned to Cu^{1+}.[S4,5] Bond-valence sum (BVS) value of Cu ion in **1** was estimated to be 1.15.[S6] And in checkCIF/PLATON report, it also gave 'PLAT794_ALERT_5_G Tentative Bond Valency for Cu1 (I). 1.19 Info.'

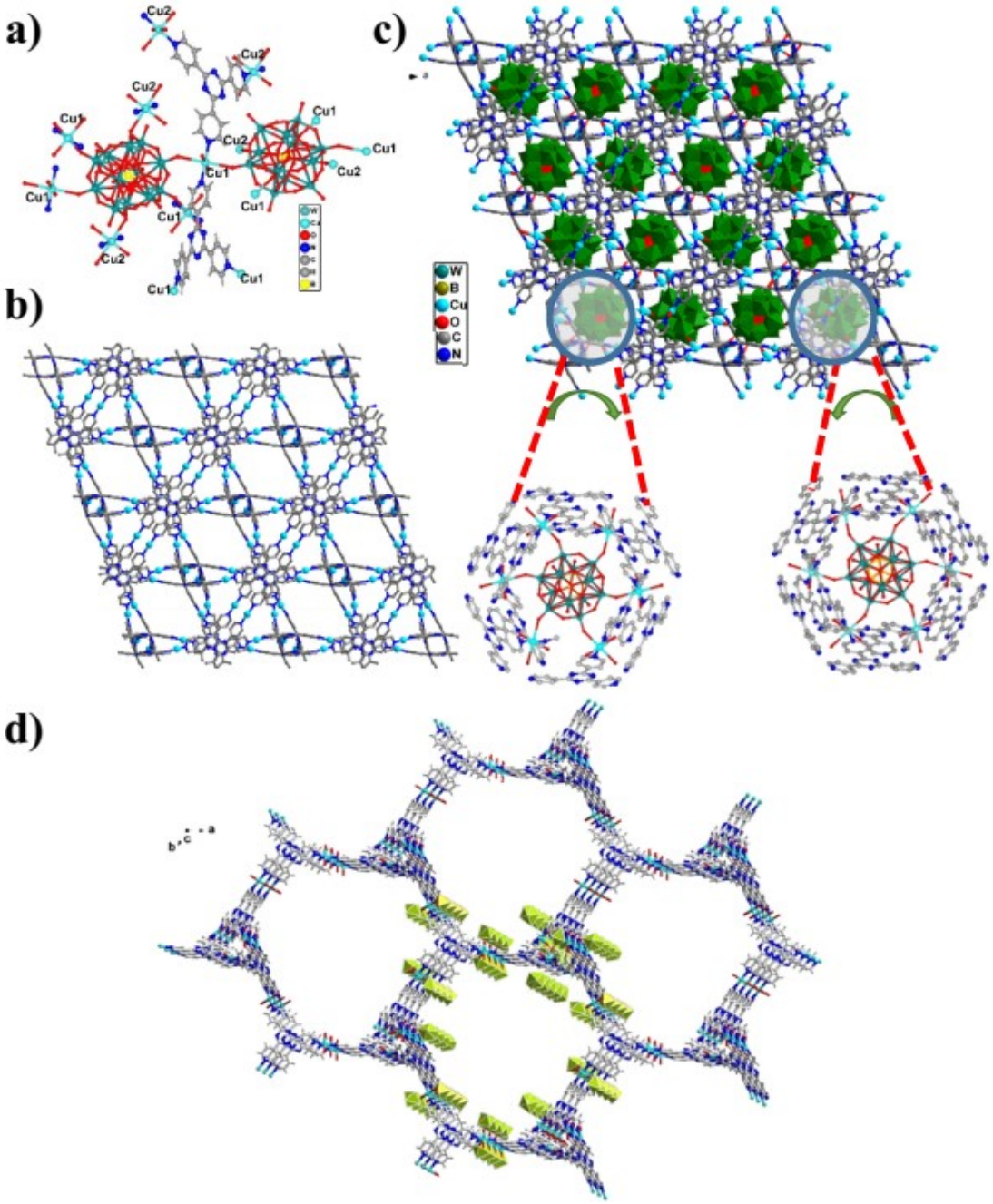

Fig. S5 (a) The coordination mode of the components of **1**. (b) The 3D framework of **1** with POMs omitted. (c) The 3D framework of **1** and the coordination modes of POMs. (d) The display of 3D structure along *c* axis (POMs are clarified).

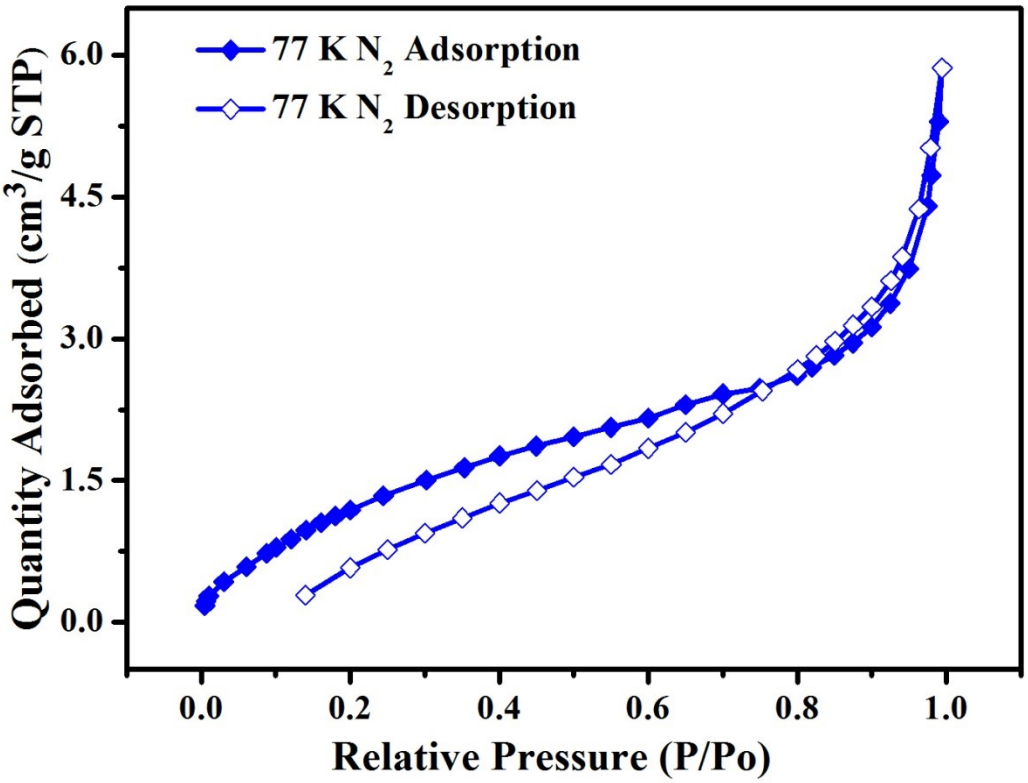

Fig. S6 The N_2 sorption isotherms of **1** at 77 K.

To demonstrate the potential of the **1** in N_2 gas absorption, we measured the adsorption isotherm of N_2 at 77 K with a desolvated sample of **1**. The BET surface area of 1 is 5.6410 m^2 g^{-1}. The N_2-adsorption capacity of **1** is lower than that of some other reported MOFs. The main reason for the low gas uptake is presumably the presence of POM in channel **1**, which occupied a large portion of void space and thus decreased the accessible pore volume.

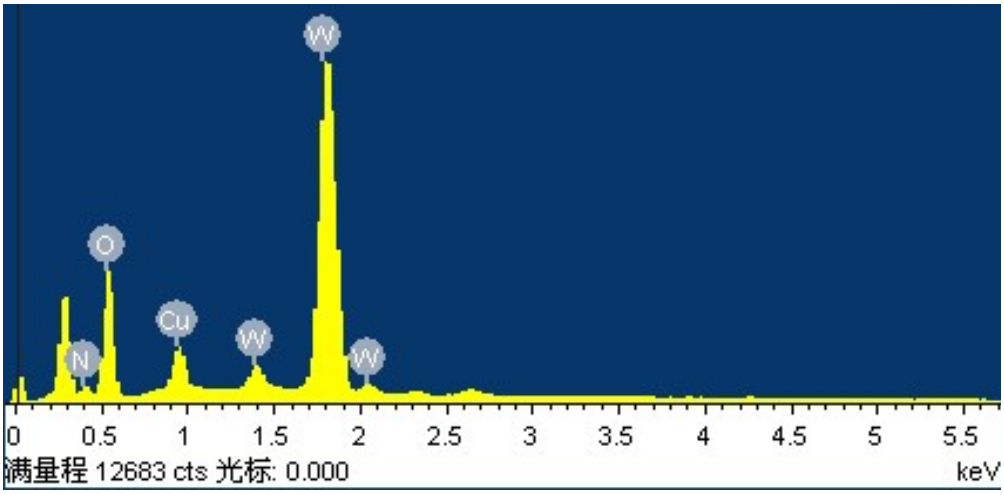

Fig. S7 The EDX spectra of **1**.

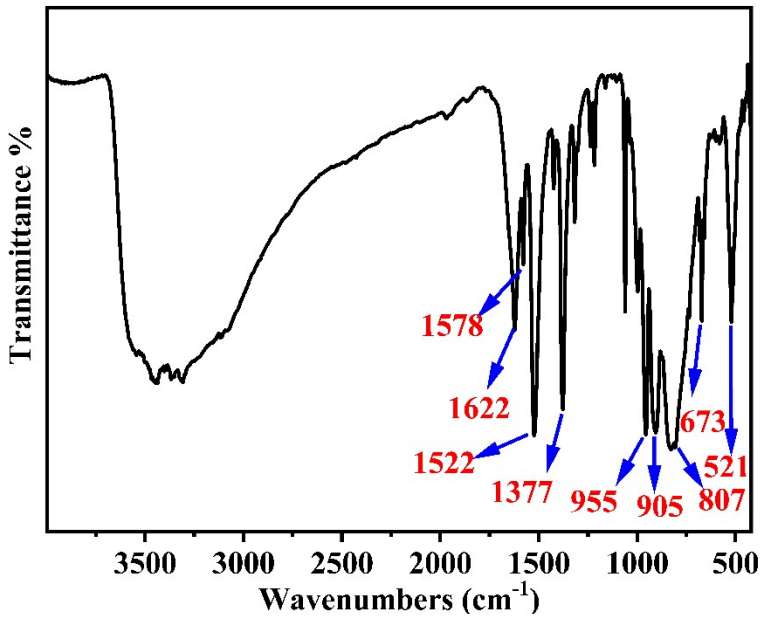

Fig. S8 The IR spectrum of **1**.

The resonances at 1000~800 cm^{-1} corresponded to O−W−O, W=O and B-O stretching vibrations. The resonances at 1622~1522 cm^{-1} are corresponding to the stretching vibrational absorption of C=C and C=N of TPT. And the peaks at 1372, 700~500 cm^{-1} are ascribed to the vibrational absorption C-H.[S7]

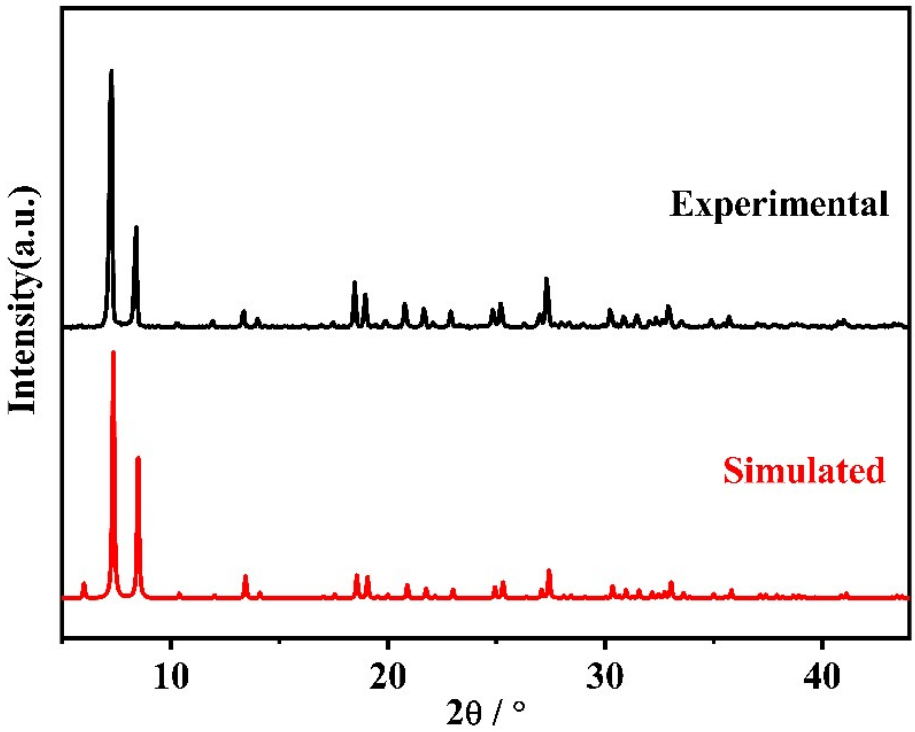

Fig. S9 The PXRD patterns of **1** (top- Experimental; bottom-Simulated).

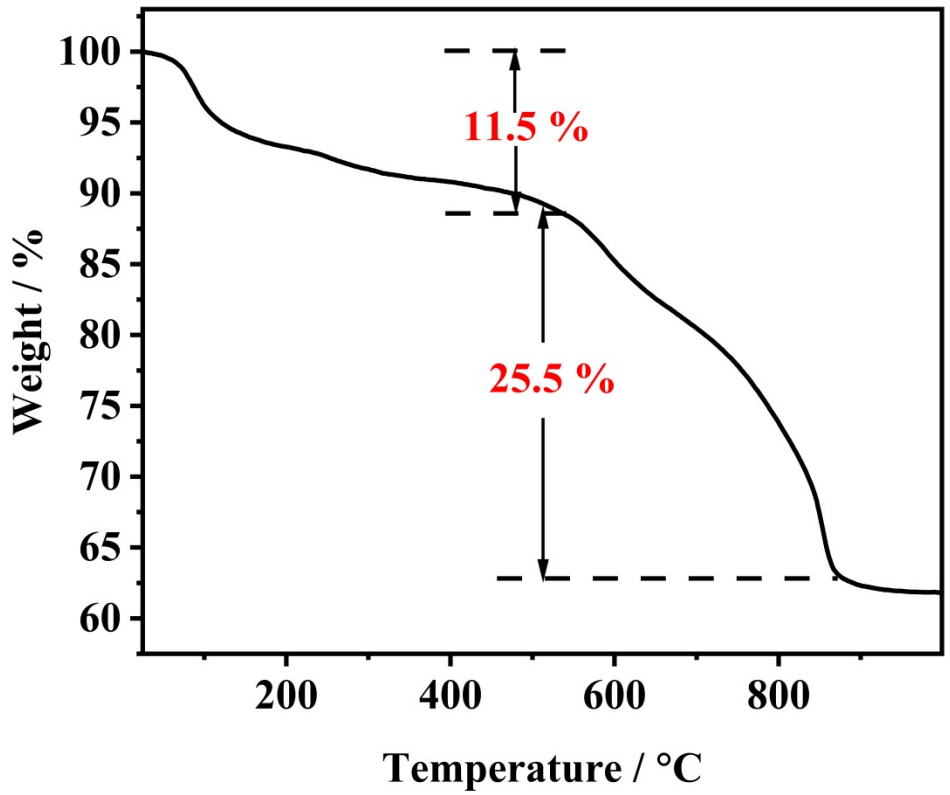

Fig. S10 The thermogravimetric analysis (TGA) curve of **1**.

In order to examine the thermal stability, thermogravimetric analysis (TG) was performed in flowing N_2 atmosphere from 25 °C to 1000 °C with a heating rate of 10 °C min^{-1} on the pure samples of **1.** The TGA curve of **1** indicates that the weight loss can be divided into two steps. The first weight loss of 11.5 % during the first step from 25 to 537 °C involves the loss of 28 lattice water molecules (calcd 11.77%). The second continuous weight loss of 25.5% among 537 to 875 °C is ascribed to the escaping of six coordinated water molecule (calc. 2.523%), the loss of two TPT ligands (calc. 14.58%), and partial decomposition of POM. The TGA of **1** reveals the framework with high thermal stability, which satisfies the prerequisite of heterogeneous catalysis.

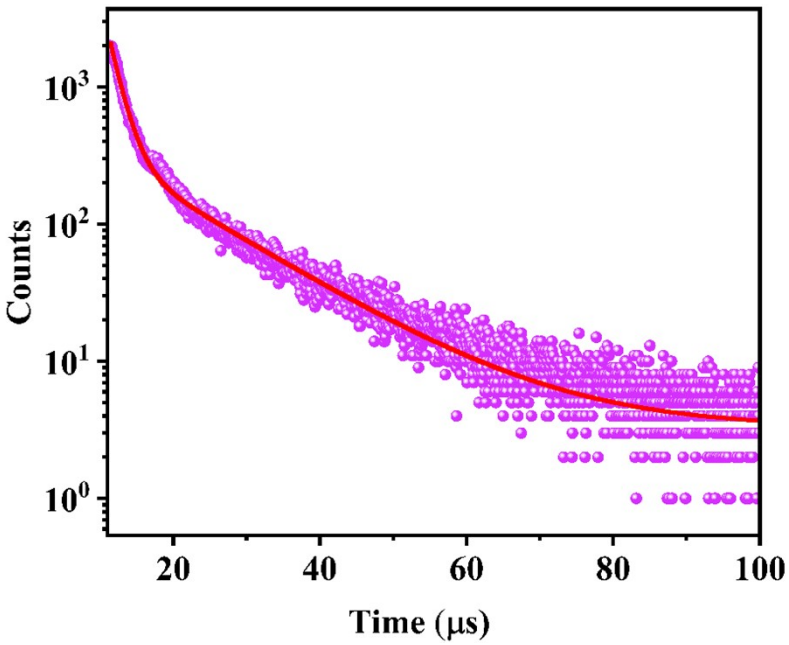

Fig. S11 The luminescence decay curve of **1**.

The lifetime curve of **1** was fitted with a double exponential function and the luminescence lifetimes τ_1 and τ_2 were 1.65 μs (44.36 %) and 9.62 μs (55.64 %), respectively, and the agreement factor was 0.998. The luminescence of **1** has an average lifetime of around 6.08 μs at room temperature.

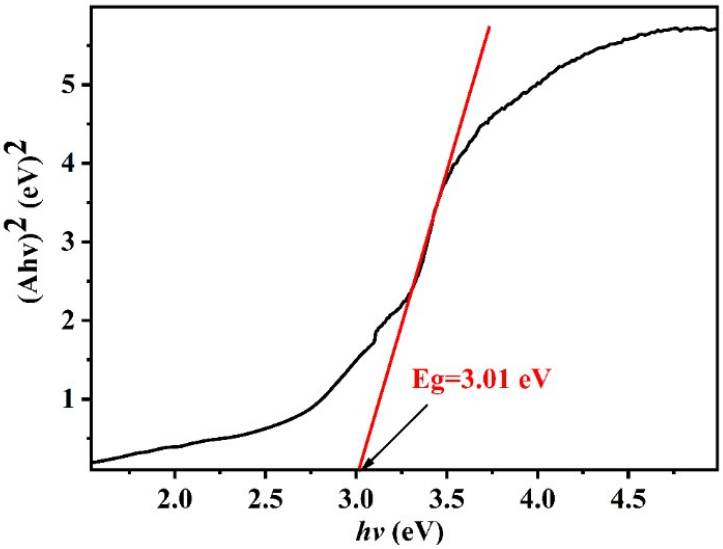

Fig. S12 The Tauc plot of **1**.

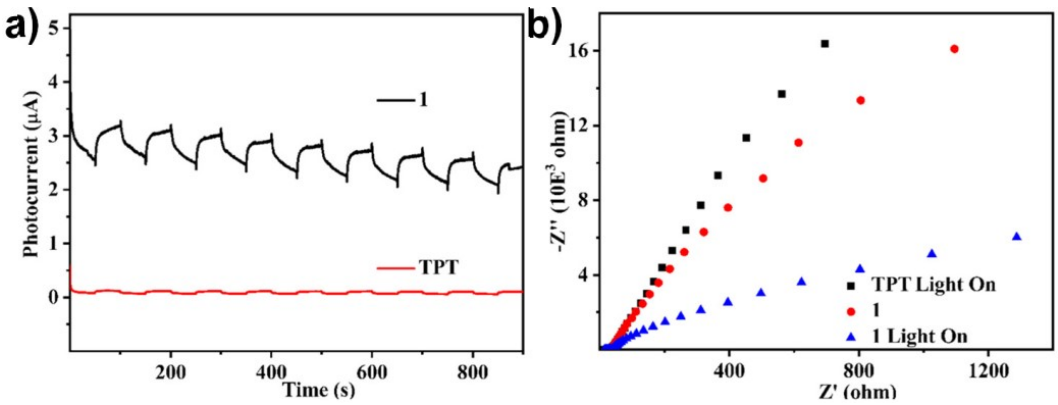

Fig. S13 (a) Transient photocurrent response. (b) Electrochemical impedance spectroscopy (EIS) Nyquist plots.

Photocatalytic oxidation of ethylbenzene

The photocatalytic process was taken on a photoreactor (WP-TEC-1020HSL, Wattecs Lab Equipment Co., Ltd.) with continuous cooling water equipment. In a typical reaction system, a 15 mL quartz tube equipped with a stir bar was charged with 10 mg of **1**, 0.5 mmol of ethylbenzene, 0.5 mL H_2O, and 2 mL CH_3CN. The resulting mixture was allowed to react in 1 atm of O_2. A 10 W 365 LED lamp was used as the light source by bottom irradiation. The quartz tube was placed ~0.45 cm from the light. The temperature of the reaction was in the range of 25 ± 5 °C. After 48 h of reaction, the mixture was centrifuged to remove 1. Then, extracted with dichloromethane, dry with Na_2SO_4, and then dried at 40°C. the conversion and selectivity were confirmed by a gas chromatography (GC) analysis and ^{1}H NMR.

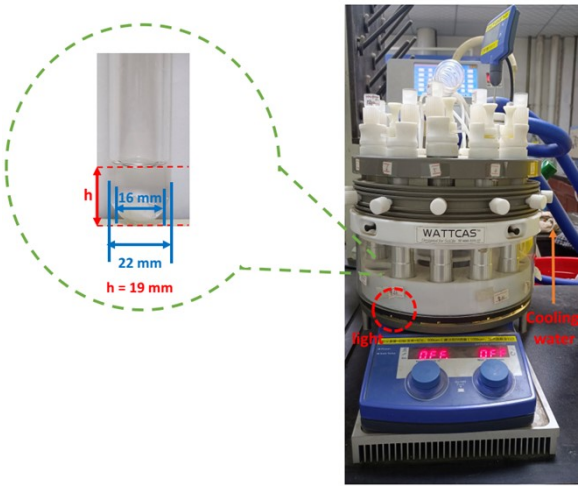

Fig. S14 The sketch portrays the reaction setup.

Active trapping experiments.

The active trapping experiments were conducted under general reaction conditions by adding 0.2 mmol of different types of radical scavengers to understand the role of radical species involved in photocatalytic ethylbenzene oxidation. Among them, 2,2,6,6-Tetramethylpiperidine (TEMPO) as a radical scavenger. KI, $AgNO_3$, butylated hydroxytoluene (BHT), and p-Benzoquinone (BQ) as scavengers for photogenerated holes, photogenerated electrons, carbon-centered radicals, and superoxide radicals, respectively.

Table S2 Summary of the activity of photocatalytic ethylbenzene oxidation.

Catalyst	Light source(temperature)	Oxidant	solvent	Yield (%)	Ref
p-BiOBr	λ＞400 nm	1 atm O_2	H_2O/*t*-BuOH	93.1	S8
POM[Fe]	10 W blue LED	1 atm O_2	acetone	63	S9
Fe_n/NC	35 ℃	TBHP	H_2O	95	S10
NCNTs	155 ℃	TBHP/O_2	CH_3CN	33	S11
1	365 nm LED	1 atm O_2	CH_3CN/H_2O	＞99	This work

Table S3 Photocatalytic oxidation of ethylbenzene under different conditions.[a]

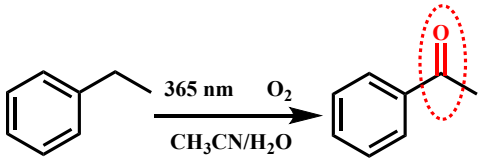

Entry	Catalyst	Atm	Conv.(%)[b]	Sel.(%)[b]
1	**1**	O_2	70.6 (24 h)	99
2	**1**	O_2	99 (48 h)	99
3	**1**	N_2	N.D.	-
4[c]	**1**	O_2	40	99
5	TPT	O_2	30	99
6	POM	O_2	6.9	99
7	$Cu(NO_3)_2$	O_2	N.D.	–
8	TPT/POM/$Cu(NO_3)_2$	O_2	36	99
9[d]	**1**	O_2	N.D.	–
10[e]	**1**	O_2	23.8	99
11[f]	–	O_2	N.D.	–

[a]Reaction conditions: 15 mg catalyst, 0.5 mmol ethylbenzene, 2 mL CH_3CN, 0.5 mL H_2O, RT, O_2 (1 atm). [b]Conversion and selectivity were determined by GC–MS and GC. [c]Without water. [d]Without light. [e]White light. [f]Without catalyst. N.D. = not detected.

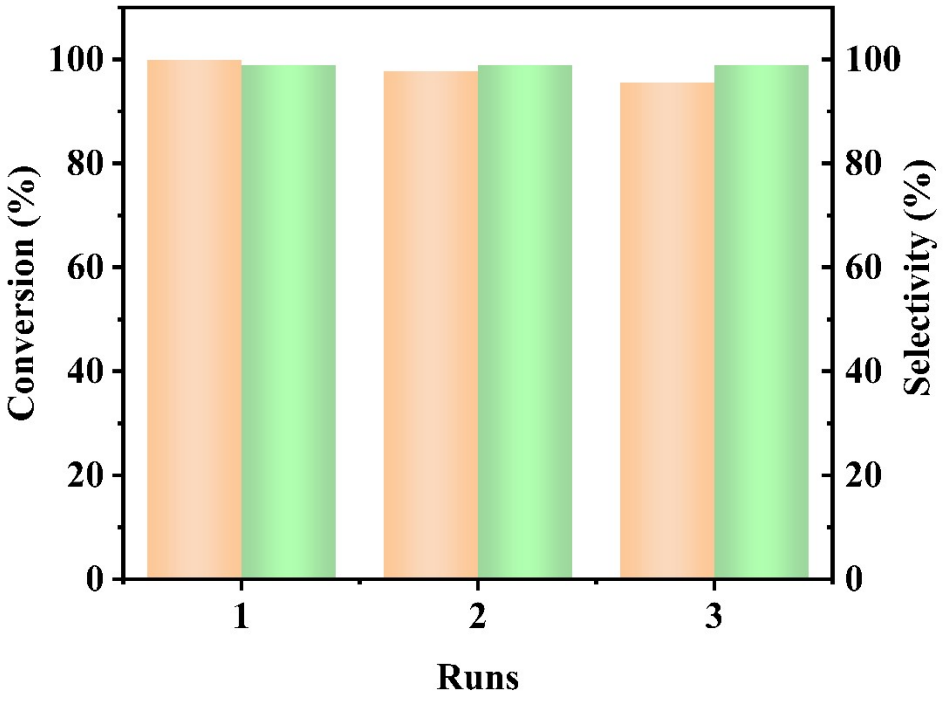

Fig. S15 Recyclability of catalyst **1**.

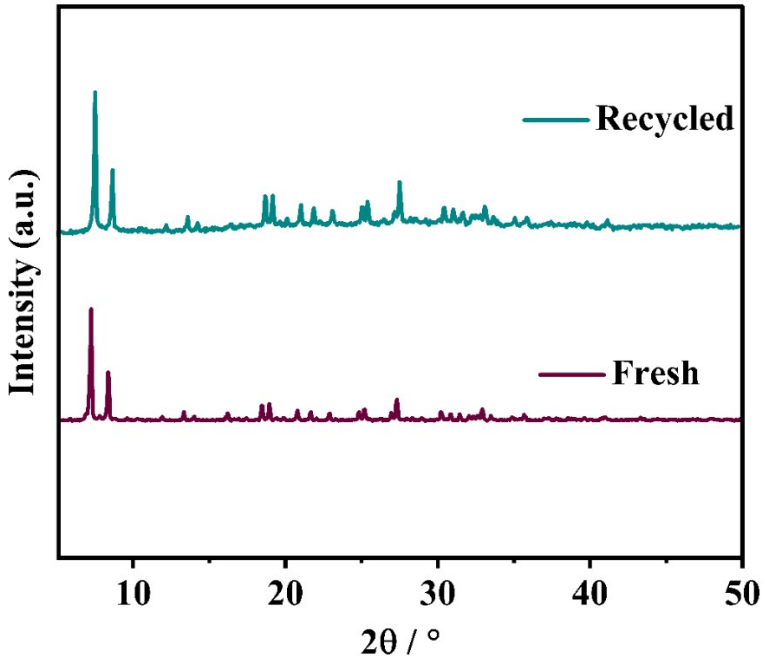

Fig. S16 The PXRD pattern of the after 3rd catalytic reaction for **1**.

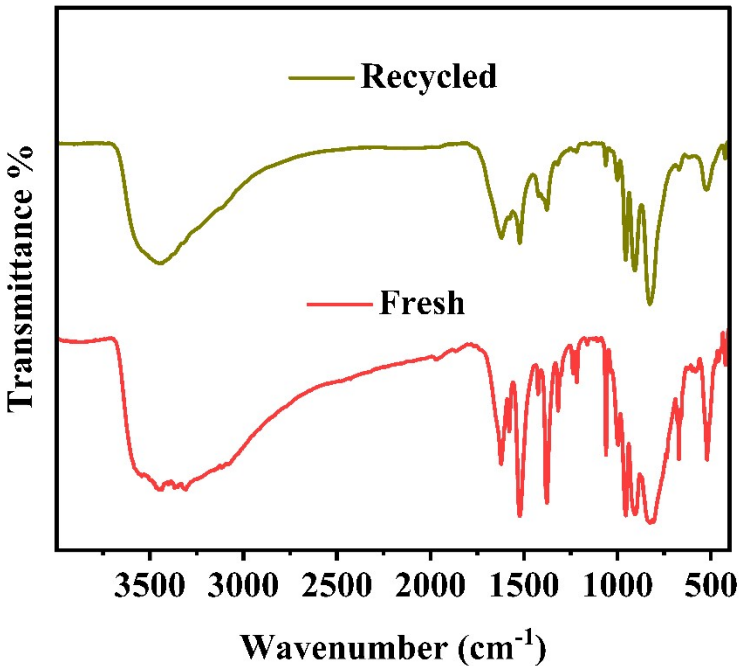

Fig. S17 The FTIR spectra of recycled **1** after three runs.

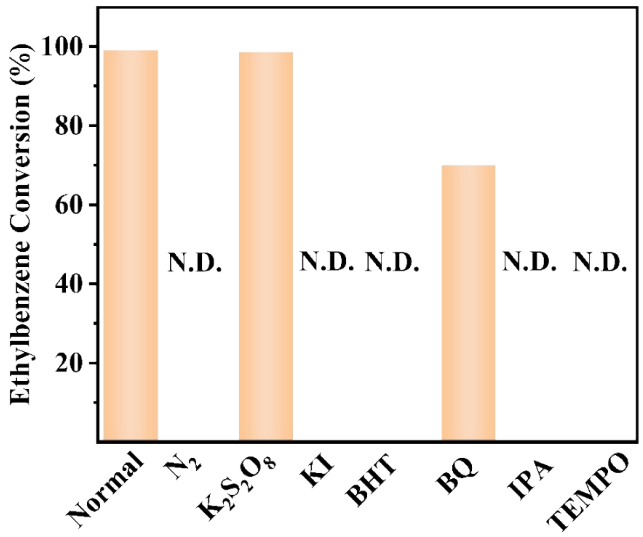

Fig. S18 Ethylbenzene conversion comparison under different active sacrificial trapping agents.

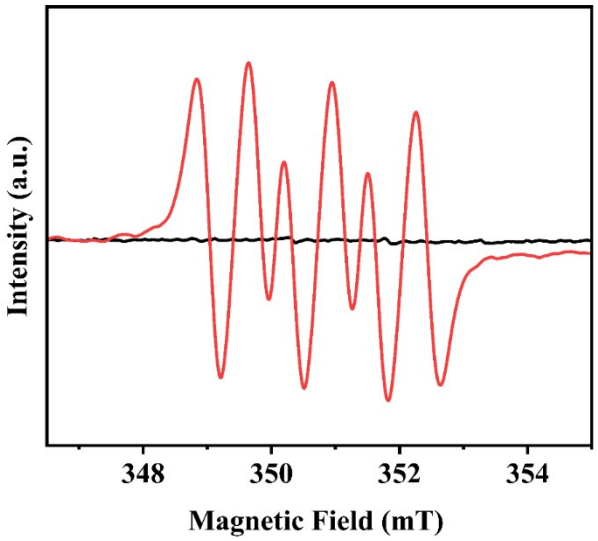

Fig. S19 The EPR spectra of superoxide radical trapped by DMPO (air).

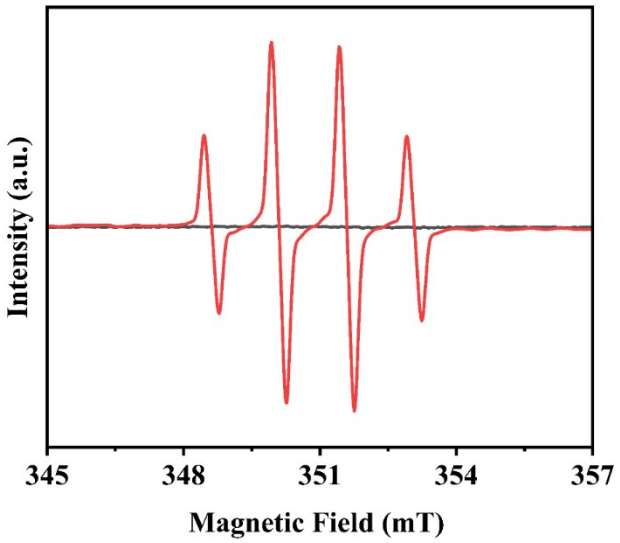

Fig. S20 The EPR spectra of hydroxyl radical trapped by DMPO (air).

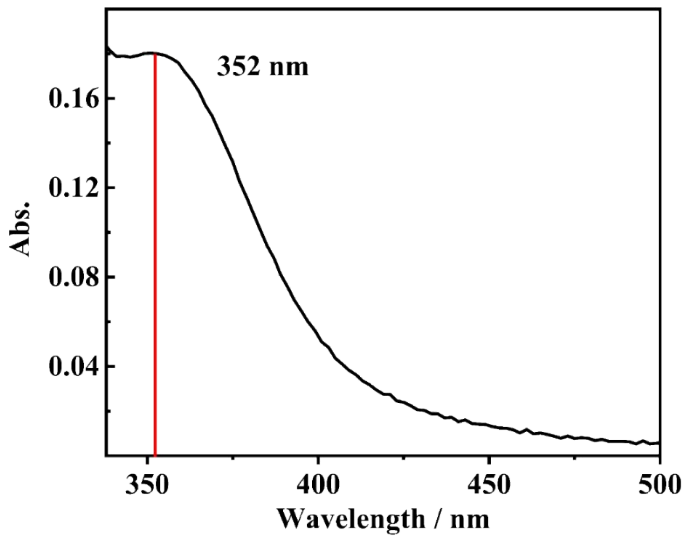

Fig. S21 The UV-Vis absorption spectrum for H_2O_2 detection over **1** by iodometry.

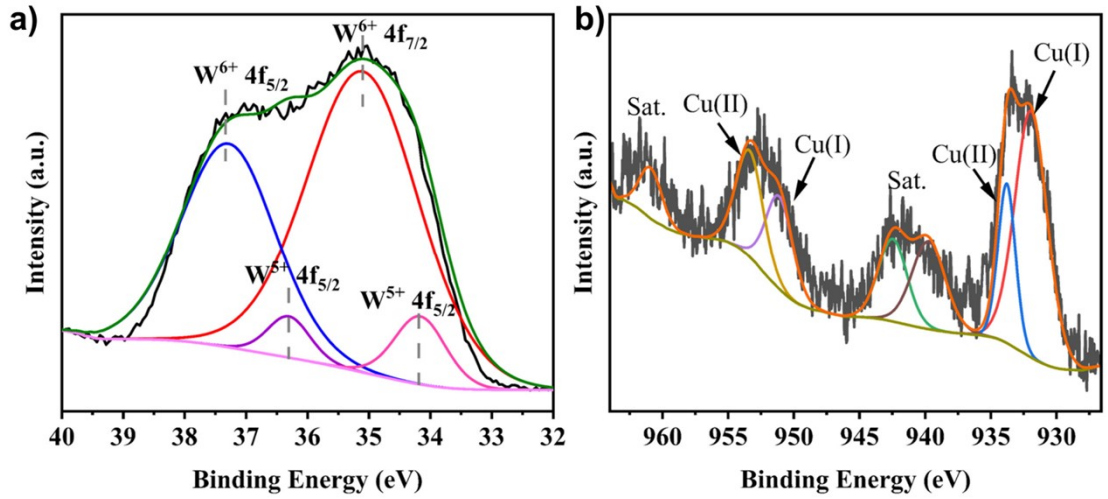

Fig. S22 The XPS spectra of W in the colored state (a) of Cu in the colored state (b).

The dominant peaks at 37.4 and 35.2 eV can be assigned to the emission of W 4f5/2 and W4f7/2 core levels from the atoms with W^{6+}, while the other two weaker peaks located at 36.3 and 34.2 eV correspond to W^{5+}.[S12] The shoulder of the colored states XPS spectrum of Cu at 932.4 eV, 933.8 eV, 951.7 eV, and 953.4 eV indicates that Cu (I) is partially oxidized to Cu (II).[S13, 14]

^{1}H NMR, GC-MS, and GC spectra of products.

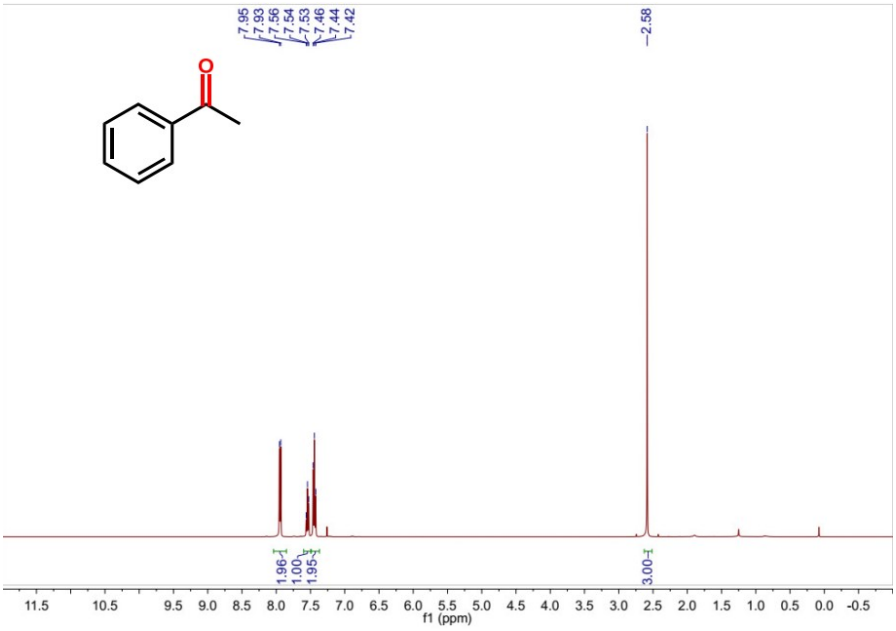

Fig. S23 ^{1}H NMR spectra of photocatalytic oxidation of ethylbenzene by **1**.

^{1}H NMR (400 MHz, $CDCl_3$) δ 7.94 (d, J = 7.6 Hz, 1H), 7.54 (t, J = 7.2 Hz, 1H), 7.44 (t, J = 7.7 Hz, 1H), 2.58 (s, 2H).

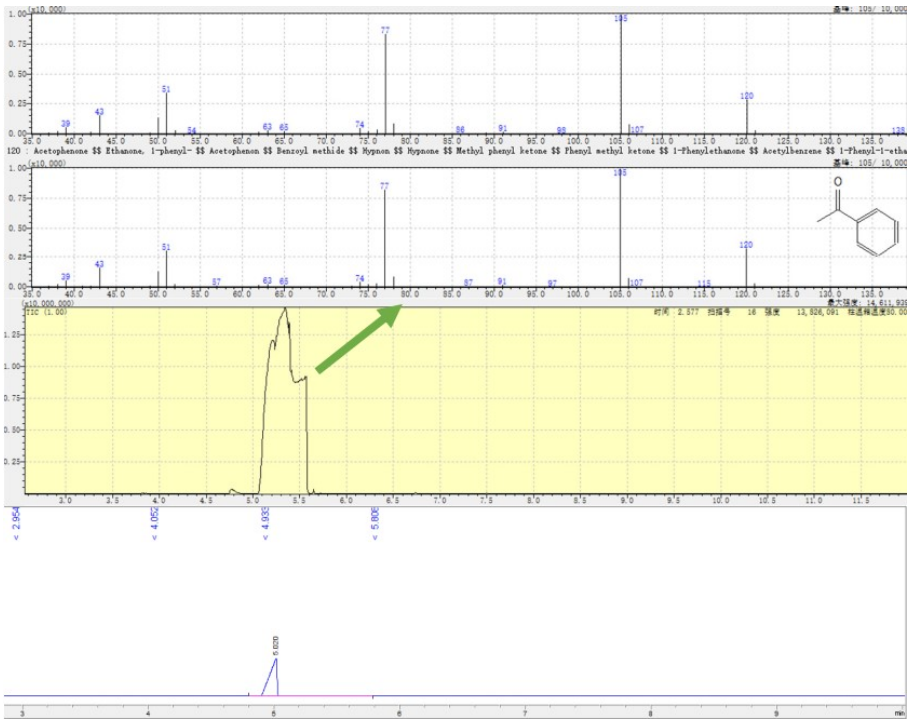

Fig. S24 GC-MS and GC of photocatalytic oxidation of ethylbenzene by **1**.

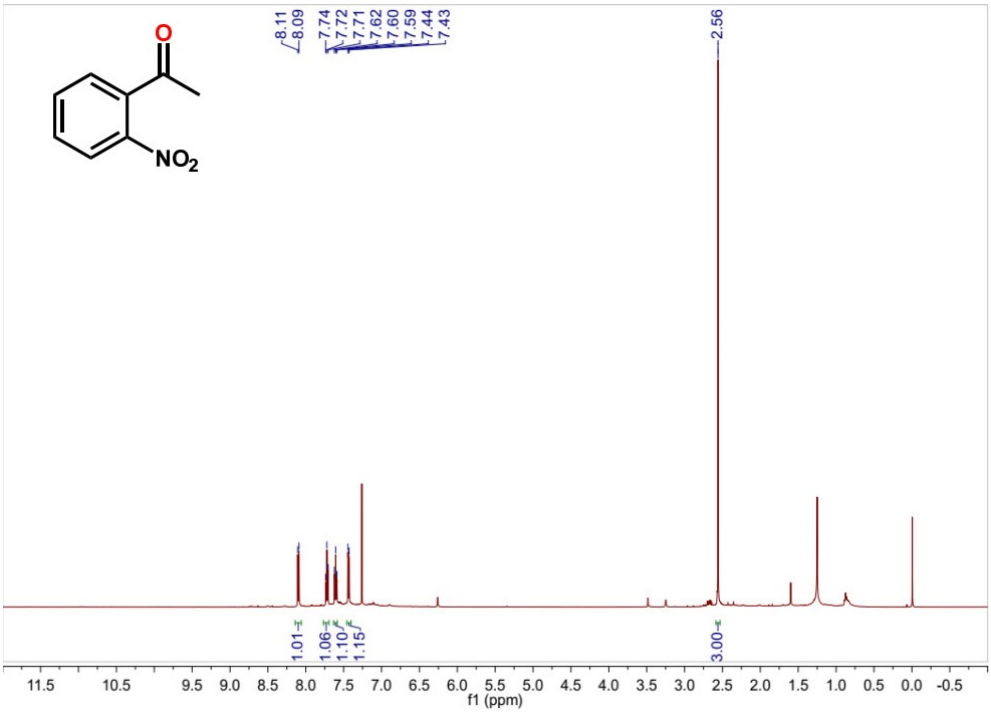

Fig. S25 ^{1}H NMR spectra of photocatalytic oxidation of 1-Ethyl-2-nitrobenzene by **1**.

^{1}H NMR (500 MHz, $CDCl_3$) δ 8.10 (d, J = 8.2 Hz, 1H), 7.72 (t, J = 7.9 Hz, 1H), 7.60 (t, J = 8.5 Hz, 1H), 7.44 (d, J = 7.5 Hz, 1H), 2.56 (s, 3H).

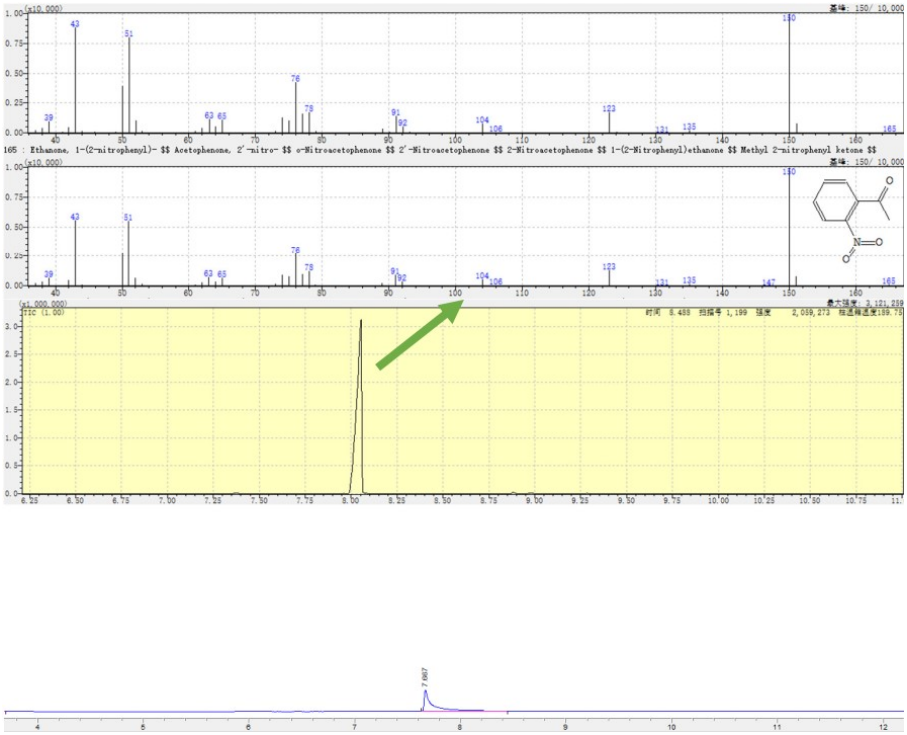

Fig. S26 GC-MS and GC of photocatalytic oxidation of 1-Ethyl-2-nitrobenzene by **1**.

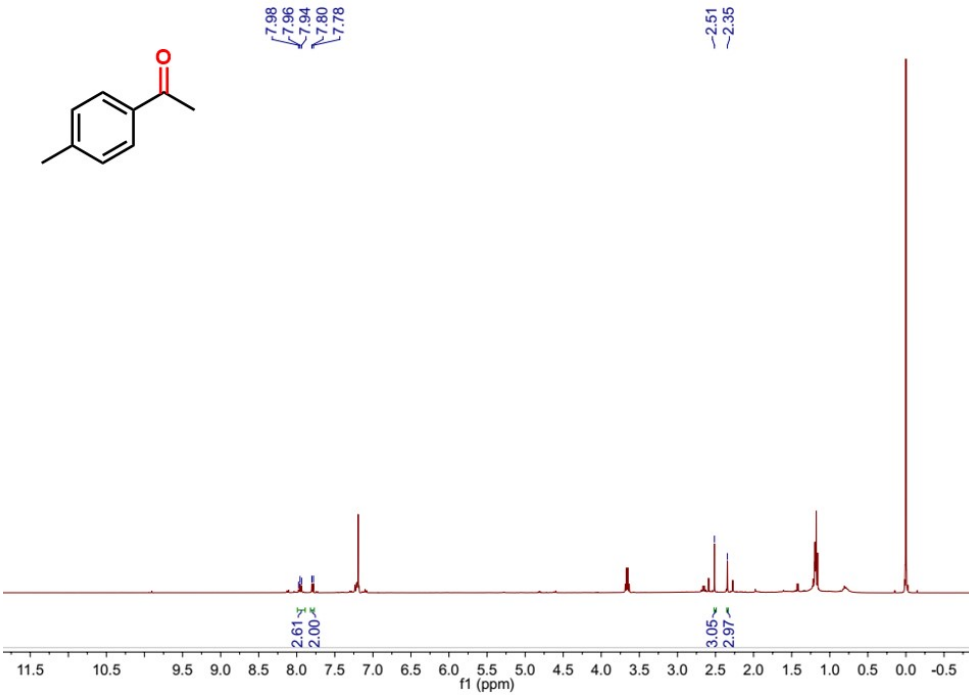

Fig. S27 [1]H NMR spectra of photocatalytic oxidation of 4-Methylphenethylamine by **1**.

[1]H NMR (400 MHz, $CDCl_3$) δ 7.96 (t, *J* = 8.0 Hz, 2H), 7.79 (d, *J* = 8.2 Hz, 2H), 2.51 (s, 3H), 2.35 (s, 3H).

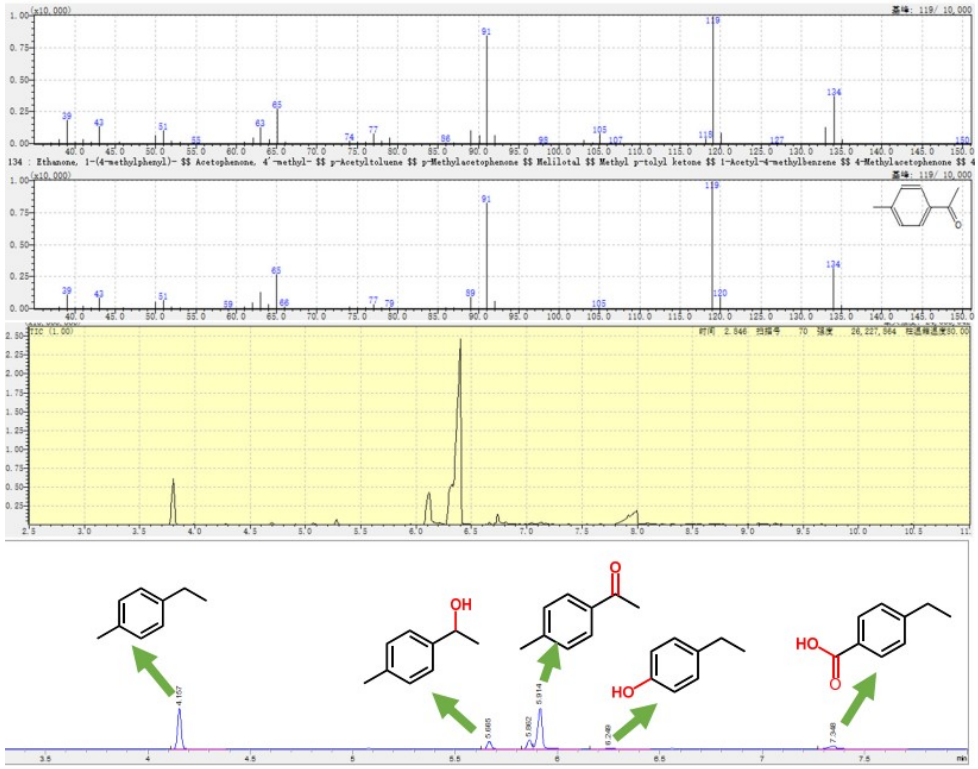

Fig. S28 GC-MS and GC of photocatalytic oxidation of 4-Methylphenethylamine by **1**.

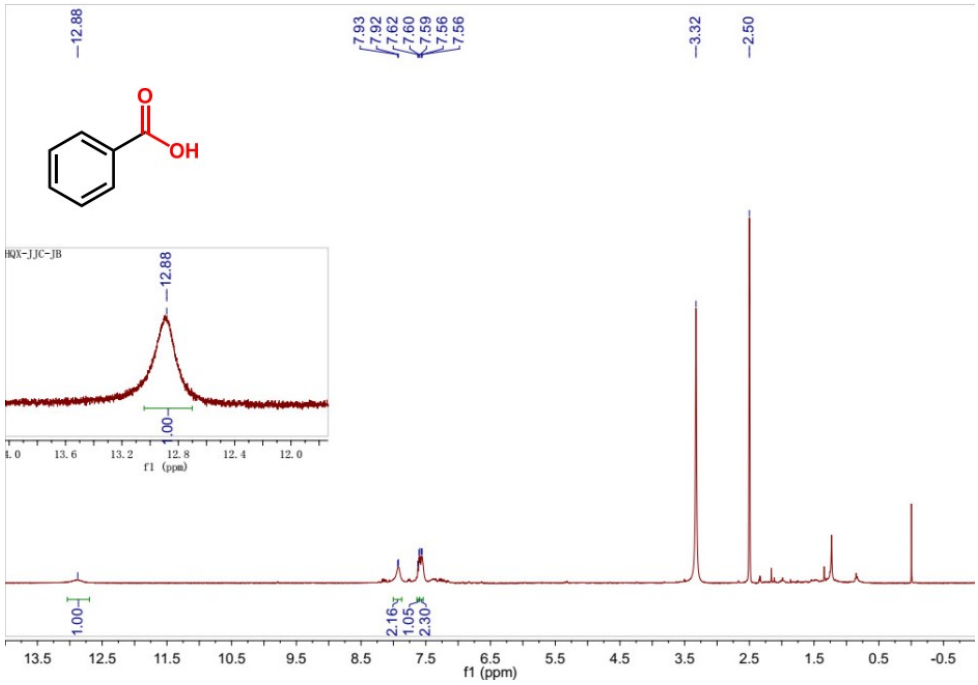

Fig. S29 ^{1}H NMR spectra of photocatalytic oxidation of toluene by **1**.

^{1}H NMR (400 MHz, DMSO) δ 12.88 (s, 1H), 7.93 (d, *J* = 4.5 Hz, 2H), 7.61 (d, *J* = 7.7 Hz, 1H), 7.59 – 7.54 (m, 2H).

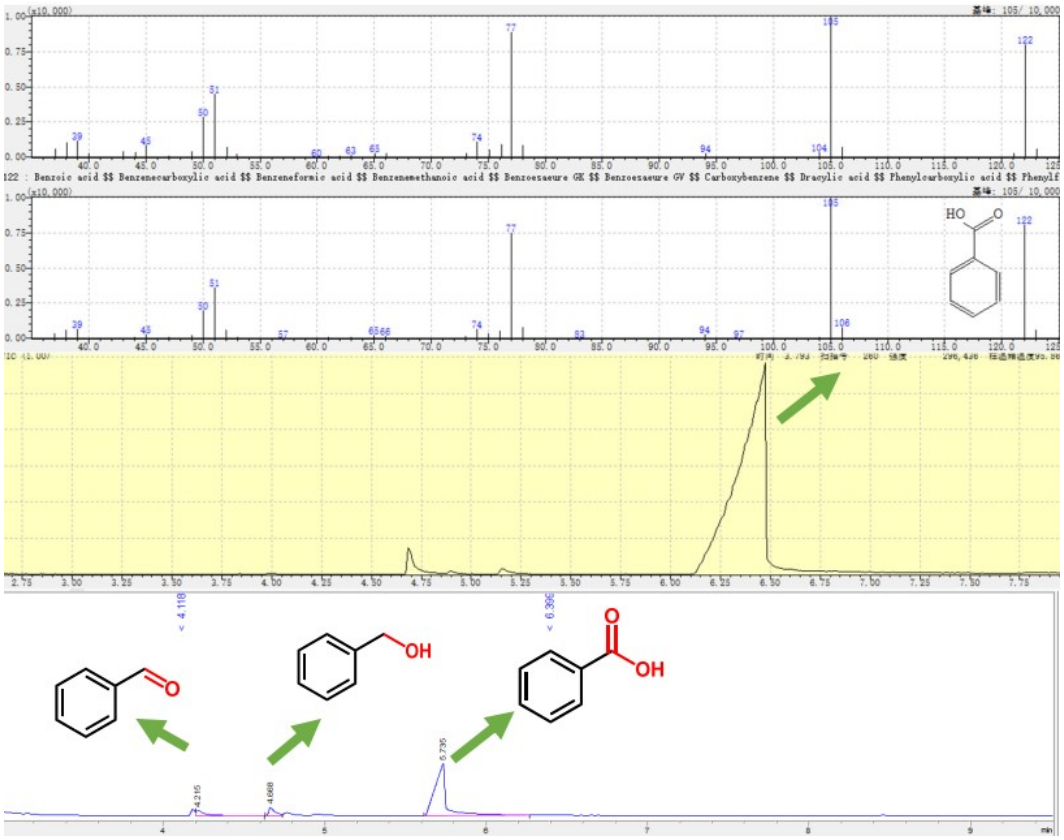

Fig. S30 GC-MS and GC of photocatalytic oxidation of toluene by **1**.

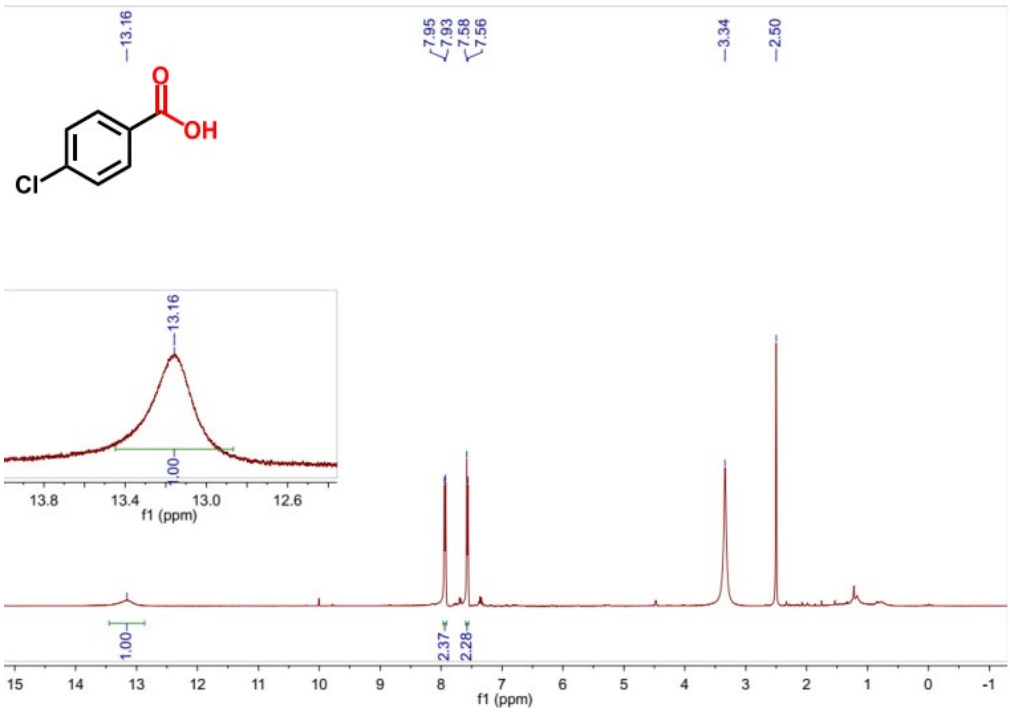

Fig. S31 [1]H NMR spectra of photocatalytic oxidation of 4-Chlorotoluene by **1**.

[1]H NMR (400 MHz, DMSO) δ 13.16 (s, 1H), 7.94 (d, J = 8.3 Hz, 2H), 7.57 (d, J = 8.1 Hz, 2H).

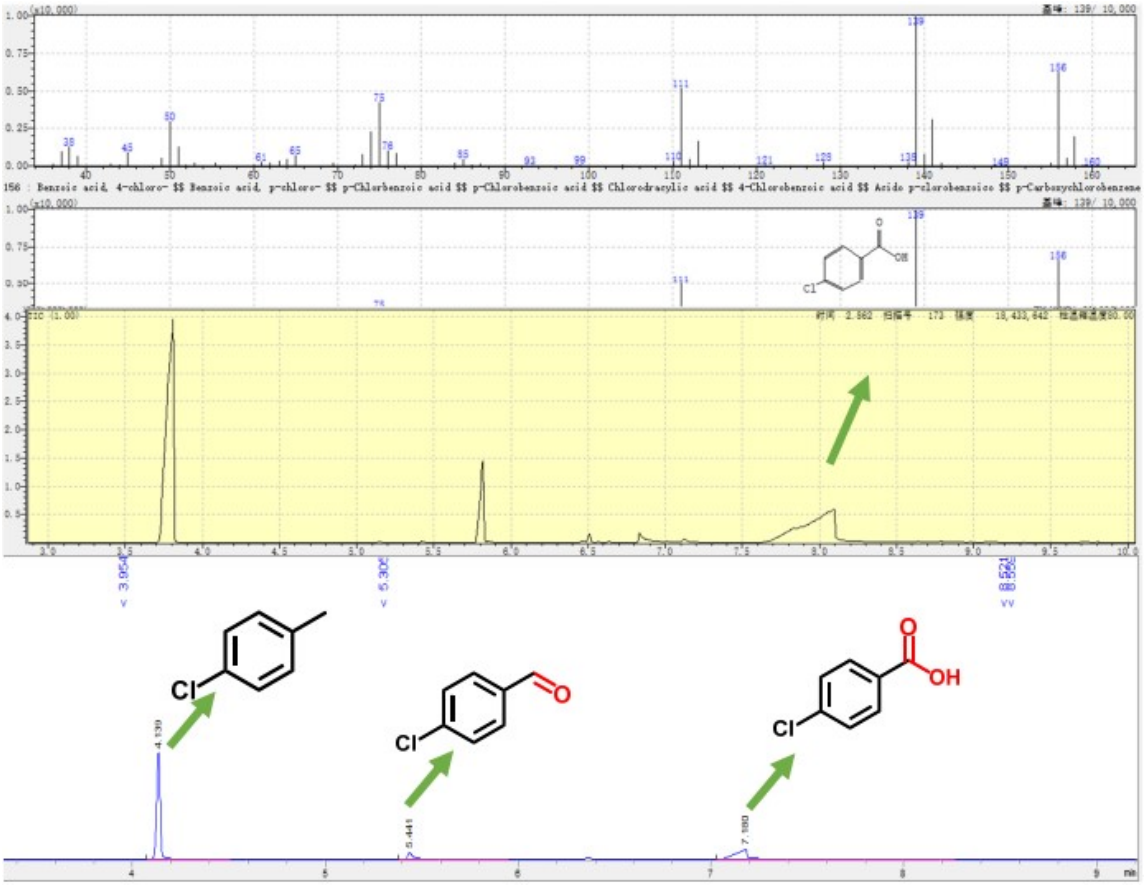

Fig. S32 GC-MS and GC of photocatalytic oxidation of 4-Chlorotoluene by **1**.

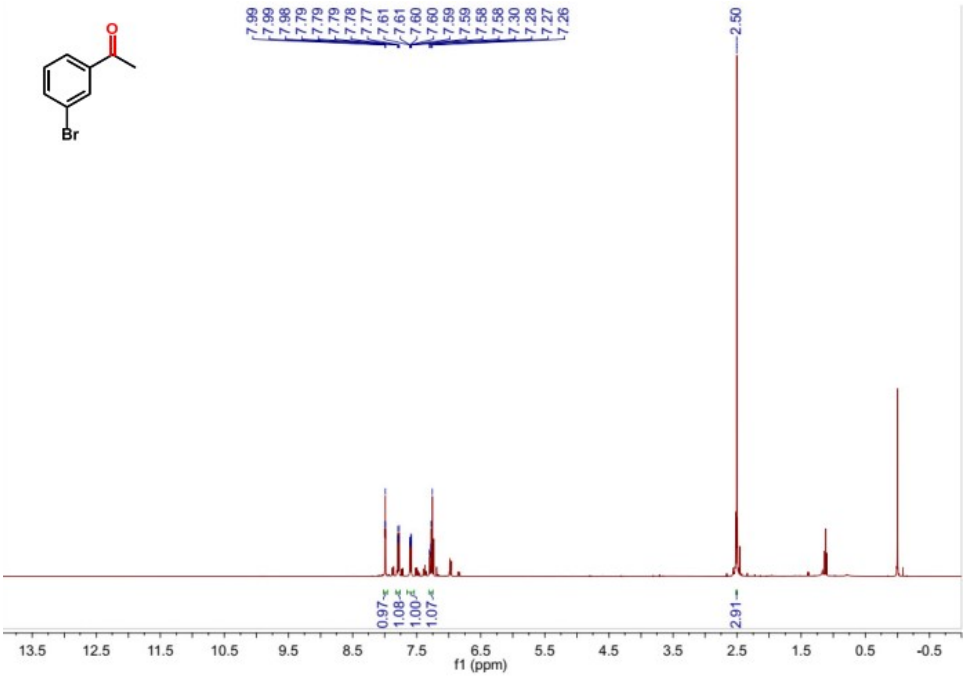

Fig. S33 ^{1}H NMR spectra of photocatalytic oxidation of 1-Bromo-3-ethylbenzene by **1**.

^{1}H NMR (400 MHz, $CDCl_3$) δ 7.99 (t, *J* = 1.8 Hz, 1H), 7.80 – 7.76 (m, 1H), 7.59 (ddd, *J* = 7.9, 1.8, 0.9 Hz, 1H), 7.28 (dd, *J* = 10.0, 8.1 Hz, 1H), 2.50 (s, 3H).

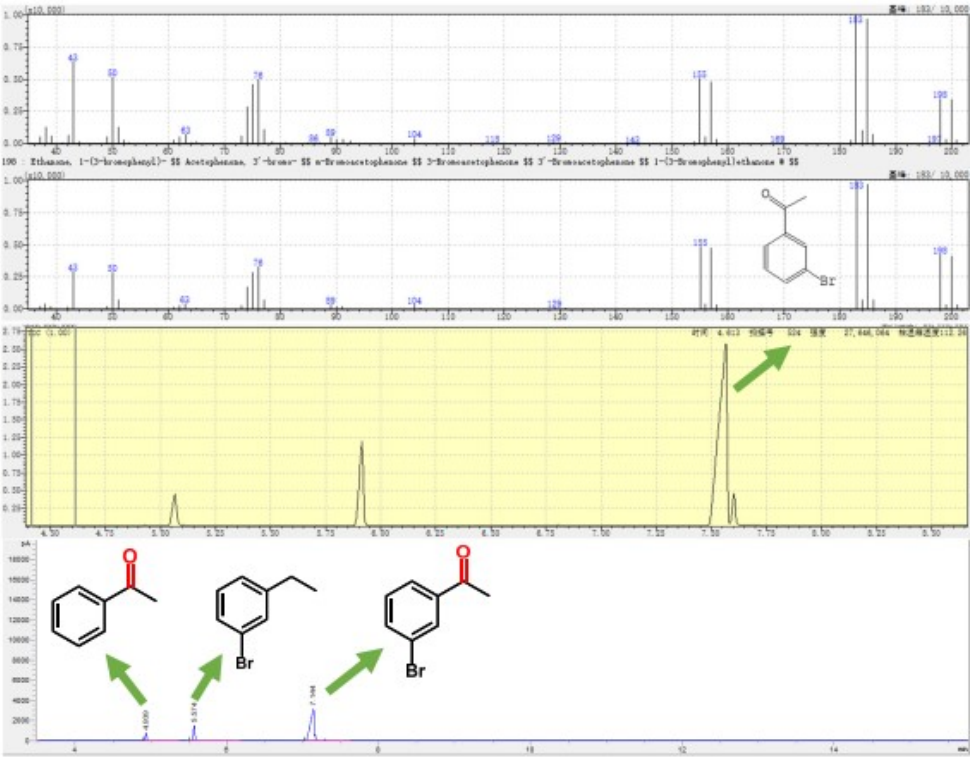

Fig. S34 GC-MS and GC of photocatalytic oxidation of 1-Bromo-3-ethylbenzene by **1**.

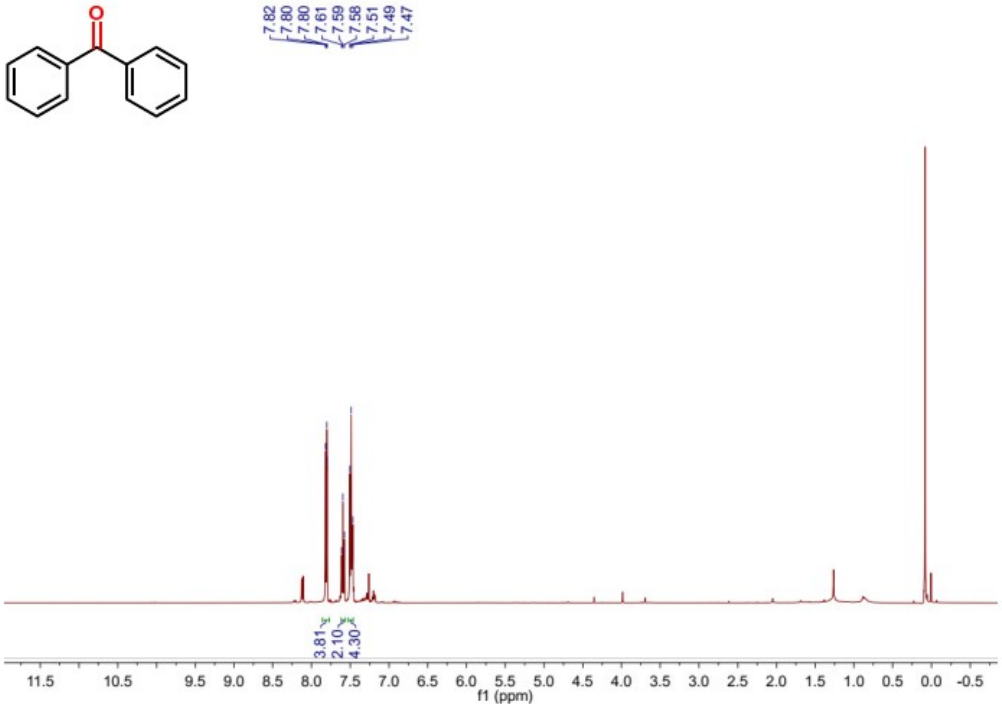

Fig. S35 ^{1}H NMR spectra of photocatalytic oxidation of Diphenylmethane by **1**.

^{1}H NMR (400 MHz, $CDCl_3$) δ 7.86–7.76 (m, 4H), 7.59 (t, J = 7.4 Hz, 2H), 7.49 (t, J = 7.6 Hz, 4H).

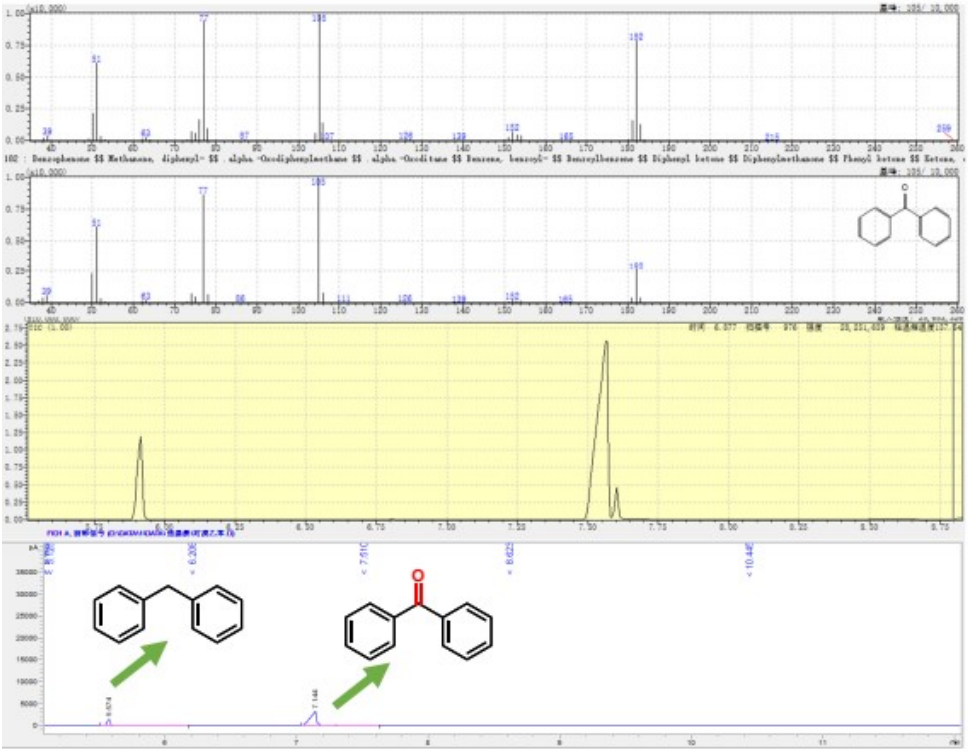

Fig S36 GC-MS and GC of photocatalytic oxidation of Diphenylmethane by **1**.

Reference

1. Q. L. Liang, N. N. Du, L. G. Gong, C. X. Wang, C. M. Wang, K. Yu and B.-B. Zhou, *New J. Chem.*, 2021, **45**, 14444–14450.

2. O. V. Dolomanov, L. J. Bourhis, R. J. Gildea, J. A. K. Howard and H. Puschmann, *J Appl Crystallogr*, 2009, **42**, 339–341.

3. Sheldrick, G.M. (2015). Acta Cryst. A71, 3-8.

4. W. Cheng, H. Zhang, D. Luan and X. W. (David) Lou, *Sci. Adv.*, 2021, **7**, eabg2580.

5. W. Zhang, L. Gong, N. Du, C. Wang, K. Yu, C. Wang and B. Zhou, *Inorg. Chem.*, 2021, **60**, 16357–16369.

6. R. S. Rarig, Jr. and J. Zubieta, *J. Chem. Soc., Dalton Trans.*, 2001, 3446–3452.

7. I. D. BROWN AND D. ALTERMATT, Acta Cryst. (1985). B41, 244–247.

8. X. Cao, A. Huang, C. Liang, H.-C. Chen, T. Han, R. Lin, Q. Peng, Z. Zhuang, R. Shen, H. M. Chen, Y. Yu, C. Chen and Y. Li, *J. Am. Chem. Soc.*, 2022, **144**, 3386–3397.

9. Y. Ma, F. Gao, W. Xiao, N. Li, S. Li, B. Yu and X. Chen, *Chinese Chemical Letters*, 2022, **33**, 4395–4399.

10. Y. Cheng, Q. Sun, L. Huang, Q. He, H. Zhang, P. Wang, Y. Zhang, S. Shi, X. Zhang, T. Gan, X. He and H. Ji, *Dalton Trans.*, 2021, **50**, 11711–11715.

11. Y. Su, Y. Li, Z. Chen, J. Huang, H. Wang, H. Yu, Y. Cao and F. Peng, *ChemCatChem*, 2021, **13**, 646–655.

12 Z.-P. Nie, D.-K. Ma, G.-Y. Fang, W. Chen and S.-M. Huang, *J. Mater. Chem. A*, 2016, **4**, 2438–2444.

13. Y. Luo, M. Wu, B. Pang, J. Ge, R. Li, P. Zhang, M. Zhou, L. Han and S. Okada, *ChemistrySelect*, 2020, **5**, 4160–4164.

14. X. Zhang, N. A. Vermeulen, Z. Huang, Y. Cui, J. Liu, M. D. Krzyaniak, Z. Li, H. Noh, M. R. Wasielewski, M. Delferro and O. K. Farha, *ACS Appl. Mater. Interfaces*, 2018, **10**, 635–641.